Structure-based enzyme inhibition mechanism studies of kaempferol and its prenylated derivatives as aldose reductase inhibitors using kinetics and molecular docking modeling

Hyun Ah Jung[1]*, Hye Eun Moon[2], Sang Ho Oh[3], Byung-Woo Kim[4], Hee Sook Sohn[1], Sook-Bae Kim[1], Jae Sue Choi [2,4]*

[1]Department of Food Science and Human Nutrition, Chonbuk National University; Jeonju 561-756, Republic of Korea

[2]Department of Food Science and Nutrition, Pukyong National University 608-737, Republic of Korea

[3]Korean BioInformation Center (KOBIC), Daejeon 305-806, Republic of Korea

[4]Blue-Bio Industry RIC, Dongeui University; Busan 614-714, Republic of Korea

*Correspondence : choijs@pknu.ac.kr; jungha@jbnu.ac.kr

*These authors contributed equally to this work

Email addresses:

HAJ: jungha@jbnu.ac.kr; HEM: mhe0306@naver.com;

SHO: sangho@kribb.re.kr; BWK: bwkim@deu.ac.kr;

HSS: hssohn@chonbuk.ac.kr; SBK: sbkim@chonbuk.ac.kr;

JSC: choijs@pknu.ac.kr

Abstract

Background: Aldose reductase inhibitors (ARIs) suppressing the hyperglycemia-induced polyol pathway have been provided as potential therapeutic candidates in the treatment and prevention of diabetic complications. It was previously reported that prenylated flavonols such as desmethylanhydroicaritin (**1**) and sophoflavescenol (**2**) from *Sophora flavescens* are promising inhibitors of rat lens aldose reductase (RLAR) and human recombinant aldose reductase (HRAR). Based upon structure–activity relationships, 3,4′-dihydroxy flavonols with a prenyl or lavandulyl group at the C-8 position and a hydroxyl or methoxy group at the C-5 position are important for AR inhibition. In order to prove the above results, a combination of computational prediction and enzyme kinetics has begun to emerge as an effective screening technique for the potential.

Results: In the present study, we predicted the 3D structure of AR in human using a docking algorithm to simulate binding between AR and prenylated flavonoids (**1** and **2**) and kaempferol (**3**) and scrutinized the reversible inhibition of AR by these proteins. Docking simulation results of **1** ~ **3** demonstrated negative binding energies (Autodock 4.0 = –9.11 to –7.64 kcal/mol; Fred 2.0 = –79.54 to –51.84 kcal/mol) and an additional hydrogen bond through Phe122 and Trp219, in addition to the previously proposed interaction of AR and phenolics through Trp20, Tyr48, His110, and Trp111 residues, indicating that the presence of 8-prenyl and 5-methyl groups might potentiate tighter binding to the active site of the enzyme and more effective AR inhibitors. Moreover, types of RLAR inhibition were different depending on the presence or absence of the 8-prenyl group, in that **1** and **2** are mixed inhibitors with

respective K_i values of 0.69 μM and 0.94 μM, while **3** showed noncompetitive inhibition with a K_i value of 4.65 μM when analyzed with Dixon plots.

Conclusion: The present study suggests that an effective strategy for screening potential AR inhibitors could be established by predicting 3D structural conformation of prenyl flavonoids and the orientation within the enzyme as well as by simultaneously determining the mode of enzyme inhibition.

Background

Long-term hyperglycemia in diabetes mellitus is considered to be the primary instigator of the pathogenesis of long term diabetic complications, including retinopathy, cataractogenesis, nephropathy, and neuropathy. To date, the pathogenesis of diabetic complication has been explained by several possible mechanisms, including increased aldose reductase (ALR2; EC 1.1.1.21)-related polyol pathway, increased advanced glycation endproduct (AGE) formation, and excessive oxidative stress [1]. ALR2 and aldehyde reductase (ALR1; EC 1.1.1.2), members of the aldo-keto reductase superfamily, are NADPH-dependent oxidoreductases that catalyze the reduction of a wide variety of aldehydes and ketones to their corresponding alcohols. In particular, ALR2 is a key enzyme in the polyol pathway that catalyzes the conversion of glucose to sorbitol in a hyperglycemic state [2]. ALR2 is found in almost all mammalian cells and at high levels in some organs, such as the lens, retina, and sciatic nerves, which are easily damaged by increased polyol pathway flux-related diabetic complications and can cause cataract [3]. Cataractogenesis is the leading cause of blindness in worldwide diabetic patients [4, 5]. Moreover, sorbitol and its metabolites accumulate in the nerves, retina, and kidneys due to their poor penetration across membranes and inefficient metabolism, resulting in the development of diabetic complications, including retinopathy, neuropathy, and nephropathy [6]. Thus, suppression of the hyperglycemia-induced polyol pathway flux by ALR2 inhibitors (ARIs) may be a potential therapeutic opportunity in the treatment and prevention of diabetic complications [7,8]. Additionally, ALR1 belongs to aldo-keto superfamily that closely resemble to ALR2 but significantly different in the C-terminal loop (297-315, 306-313) responsible for substrate and inhibitor specificity. ALR1 preferentially

metabolizes 3-deoxyglucosone and methylglyoxal, which are both reactive intermediates for AGE formation and may account for some undesirable side effects [9]. Therefore, it is necessary to exploit the specificity and selectivity of these two homologues. In particular, the ability of ALR2 to reduce excess glucose to sorbitol in diabetes mellitus has implicated the enzyme in the pathogenesis of diabetic complications affecting the eyes, kidneys, and nervous system [10].

Structure-based enzyme mechanism studies have been prominently used to elucidate the mechanism of inhibition. With respect to structural information of enzymes and inhibitors, various 3D-molecular docking programs have been developed in recent years. However, limitations have been imposed on the explanation of the enzyme/inhibitor complex, including the binding affinity of enzyme-inhibitors and enzyme-substrates, as well as reaction velocity. Therefore, kinetic studies will take advantage of supporting evidence for the predicted mechanism from molecular docking models. Two kinetic methods have been widely used to determine the type of inhibition: Lineweaver–Burk plot and the Dixon plot. The former is the double reciprocal plot [plot of 1/enzyme velocity (*1/V*) against 1/substrate concentration (1/[S])] drawn to distinguish the inhibition pattern, including competitive, non-competitive, and uncompetitive inhibition and the enzyme kinetic parameters, including K_m and V_{max} values according to the Michaelis–Menten kinetics equation. The y-intercept of such a graph is equivalent to $1/V_{max}$; the x-intercept of the graph represents $-1/K_m$. Competitive inhibitors have the same y-intercept ($1/V_{max}$) but different slopes (K_m/V_{max}) and x-intercepts (K_m) with increasing concentrations of inhibitors. In the case of mixed inhibition, the inhibitor is capable of binding to both the free enzyme and to the enzyme-substrate complex. This inhibition type is different from noncompetitive inhibition in that the dissociation constant (K_{ia}) for binding the

free enzyme may differ from the dissociation constant (K_{ib}) for binding the enzyme-substrate complex. Since the mixed inhibitor binds to the enzyme at a distinguished location from the substrate binding site, the binding of the inhibitor will either alter K_m or V_{max} or both. In other words, the apparent K_m may decrease, depending on the relative values of K_{ia} and K_{ib}. In a situation where the two K_i values are the same, the apparent K_m will be unchanged. This is called non-competitive inhibition and shows the point on the x-intercept representing $-1/K_m$ [11]. Compared with the Lineweaver-Burk plot, the Dixon plot is a single reciprocal graphical method (plot of 1/enzyme velocity (*1/V*) against inhibitor concentration [I]) used to determine the type of enzyme inhibition and is used to easily calculate the dissociation or inhibition constant (K_i) of the enzyme/inhibitor complex [12,13]. The K_i value is an indication of inhibitor potency and how tightly an inhibitor binds to enzymes; it is the concentration required to produce half of the maximum inhibition as well as the affinity between enzymes and inhibitors. Plotting $1/V$ against concentration of inhibitor [I] at various concentrations of substrate produces a group of intersecting lines. The corresponding concentration at the intersection point on the x-y plane (x-axis value) is equal to $-K_i$ value in mixed inhibition, while the value of the x-intercept implies $-K_i$ in noncompetitive inhibition.

In order to confirm RLAR inhibitory activity, prediction of the protein-ligand confirmation was carried out with two predicting programs, Autodock 4.0 and Fast Rigid Exhaustive Docking (Fred) 2.0. The programs were used to dock the inhibitors into the binding sites of the crystallographic structures of enzymes defined with all residues located 5~6 Å from the original enzyme/inhibitor complex. Currently, automated docking is widely used as an effective means of quickly and accurately predicting biomolecular conformations and binding energies of protein-ligands

complexes in molecular design. In particular, Autodock 4.0 uses a semi-empirical free energy force field to predict binding free energies of protein–ligand complexes of a known structure and binding energy for both the bound and unbound states [14]. Apart from Autodock 4.0, Fred 2.0 was also employed due to consolidated evidence including the rigid rotations and translations of each conformer within the binding site. The approach of the Fred software is to thoroughly dock the scores of all possible positions of each ligand in the binding site, exhaustively test all poses of the ligand within the defined binding site, and maintain the protein-ligand complex as rigid during most of the docking process, leading to compensation for target flexibility [15]. The highly hydrophobic active site pocket of ALR2 is formed by aromatic residues (Trp20, Tyr48, Trp79, Trp111, Phe121, Phe122 and Trp219); nonpolar residues (Val47, Pro218, Leu300 and Leu301) and polar residues (Gln49, Cys298 and His110) [1,9]. ARIs generally make use of both polar and nonpolar interactions to establish complementarity with the extended enzyme binding pocket, which is best described as comprising two regions: (1) a polar site with residues Trp20, Tyr48 (the proton donor), and His110 and the positively-charged nicotinamide moiety of $NADP^+$ and (2) a nonpolar site with residues Trp111, Thr113, Phe115, Phe122, Leu300 [8].

Prenyl-substituted kaempferols, including desmethylanhydroicaritin (**1**) and sophoflavescenol (**2**), were isolated from dried roots of *Sophora flavescens* AIT (Leguminosae, Sophorae Radix), which are well known in traditional Chinese medicine (TCM). In our previous study, *Sophora flavescens* and its prenylated flavonoids were reported to possess antioxidant [16,17], anti-diabetic, and anti-diabetic complication activities [18,19]. In particular, two prenylated flavonoids **1** and **2** exhibited RLAR inhibitory activities; however, there is no detailed information on the mode of inhibition or the enzyme-inhibitor molecular interactions. Therefore, the

aims of this study were to identify an approach to develop potent anti-diabetic complication drugs by scrutinizing molecular docking predictions and enzyme kinetics of prenylated flavonoids **1** and **2**.

Results

Enzyme kinetics in RLAR inhibition

The RLAR inhibitory activity of test flavonoids **1** ~ **3** was evaluated. Among them, sophoflavescenol (**2**) ranked with the most potent inhibitory activity with an IC_{50} value of 0.76 ± 0.04 μM, and desmethylanhydroicaritin (**1**) came in second with an IC_{50} value of 1.03 ± 0.13 μM, followed by kaempferol (**3**) with an IC_{50} value of 5.13 ± 0.05 μM. Considering individual structures of **1** ~ **3**, compound **1** harbors a prenyl group at the 8 position of the A-ring in the kaempferol skeleton; **2** possesses the additional 5-methoxy group in the A-ring of **1** (Figure 1). Under interpretation using Dixon plotting, compounds **1** and **2** showed mixed type inhibition with respective K_i values of 0.94 μM and 0.69 μM, and **3** showed noncompetitive inhibition with a K_i value of 4.65 μM (Table 1; Figure 2). Similar to the results of the Dixon plots, the lines of both **1** and **2** intersected in the left side, indicating mixed type inhibitors, while the lines of **3** show the same point on the x-intercept representing noncompetitive inhibitors in Lineweaver-Burk plots (Figure 3). The respective kinetic parameters of **1** ~ **3** were also calculated using the Lineweaver-Burk equation: $\frac{1}{V} = \left(1 + \frac{[I]}{Ki}\right)\frac{Km}{Vmax}\frac{1}{[S]} + \frac{1}{Vmax}$ and an altered equation: $V_{max\ app} = Vmax/\left(1 + \frac{[I]}{Ki}\right)$. The K_m and V_{max} values of **1**~**3** depending on the concentrations of inhibitors are presented in Table 2. In the presence of different concentrations of **1**~**3**, respective V_{max} values were decreased, but the K_m values between prenylated flavonoids (**1** and **2**) were

distinguished from those of non-prenylated flavonoid (**3**). There was no change in the K_m (40.11 mM) or K_i value (6.30 and 6.20 μM) of **3** with different concentrations of substrate, a characteristic of noncompetitive RLAR inhibition. On the other hand, the respective K_m values of **2** and **3** increased with higher substrate concentrations. As for **1**, the K_m value changed from 9.85 mM at a concentration of 0.11 μM to 12.32 mM at a concentration of 0.56 μM and the V_{max} value also decreased from 0.016 μmole/mL/min to 0.010 μmole/mL/min, depending on the inhibitor concentration. The similar enzymatic parameter mode was also detected in **2**, showing the increasing K_m values from 12.14 mM to 13.38 mM and the decreasing V_{max} values from 0.016 μmole/mL/min to 0.010 μmole/mL/min with increasing inhibitor concentrations. The above enzymatic parameters for **2** and **3** confirm a mixed RLAR inhibition. In the case of mixed type inhibition, two kinds of K_i values representing the affinity between the enzyme and inhibitor can be calculated if the inhibitors bind to enzyme alone (K_{ia}) or enzyme-substrate complexes (K_{ib}). Interestingly, the K_{ia} and K_{ib} of **1** were 0.29 and 0.74 μM, respectively, and those of **2** were 0.35 and 0.46 μM at a concentration of 0.11 μM, indicating that **2** has much greater potential for binding to not only enzyme but also enzyme/substrate complexes than does **1**.

Molecular docking model of 1~3 in RLAR inhibition

As illustrated in Figure 4, the AR-inhibitor complexes were formed with compounds **1**~**3** stably posed in the pocket of the AR in Autodock 4.0 (pink) and Fred 2.0 (blue). As for **1**, the binding site predicted by Autodock 4.0 was formed by residues Leu30; Leu301; Trp20; His110; Cys298; Phe122; Val297; Ala299; Trp111; Trp219; Val47; Pro218; Trp79, while that predicted by Fred 2.0 was formed by residues Leu300; Leu301; Trp20; His110; Ser302; Cys298; Phe122; Val297; Ala299; Trp111; Trp219; Pro218; Val47; Tyr48; Trp79. For **2**, the binding site predicted by Autodock 4.0 was

formed by residues Ser210; Cys298; Trp20; Tyr209; Phe121; Trp79; Lys21; Phe122; Gln49; Trp111; Trp219; His110; Val47; Tyr48; Ser22; Asn50, while that predicted by Fred 2.0 was formed by residues Leu300; Ser210; Cys298; Trp20; Tyr209; His110; Ser302; Asn160; Phe122; Cys303; Glu185; Gln49; Leu301; Trp111; Trp219; Val47; Tyr48; Trp79. In the case of **3**, the binding site predicted by Autodock 4.0 was formed by residues Leu17; Ser210; Cys298; Asp43; His110; Asp216; Thr19; Trp111; Lys77; Ser214; Trp20; Tyr209; Gly18; Asn160; Pro261; Gln183; Lys262; Pro211; Pro215; Ser159; Tyr48; Ile260; Gly213; Lys21, while that predicted by Fred 2.0 was formed by residues Leu17; Ser210; Cys298; Asp43; His110; Asp216; Thr19; Trp111; Lys77; Ser214; Trp20; Tyr209; Gly18; Asn160; Pro261; Gln183; Lys262; Pro211; Pro215; Ser159; Tyr48; Ile260; Lys21. Due to the similarity in flavonoid structure, it was observed that test compounds **1**~**3** interacted with AR through well-known active sites, such as hydrophobic and polar residues [1,8]. Due to the presence of a prenyl group, **1** and **2** might interact with ALR2 via a specific and additional nonpolar site, including that of the Leu300 and Phe122 residues which are not present in **3** (Figure 4). In addition to the active site residue, the docking analysis also showed that the respective docking energies of **1**~**3** were –7.94, –7.64, –9.11 kcal/mol according to Autodock 4.0 and –51.84, –57.27, –79.50 kcal/mol according to Fred 2.0, when accounting for the lowest energy conformation of the most predicted complex. This result indicated that **1**~**3** bound tightly at the active site.

Discussion

The International Diabetes Federation has recently noted that a staggering 366 million people around the world are struggling with either type I or II diabetes. In particular,

type II diabetes is a leading health concern due to its escalating prevalence rate throughout the world and its associated serious diabetic complications. Moreover, high morbidity and mortality rates associated with chronic diabetic complications make the disease the third largest killer after cancer and cardiovascular disease [20]. The disease is taking a deadly toll, causing 4.6 million deaths each year. There has been a growing demand for the treatment and prevention of diabetes and diabetic complications. In particular, ALR2, a key enzyme in the polyol pathway is reported to be highly implicated in the pathogenesis of diabetic complications. Thus, AR reduction of the hyperglycemia-induced polyol pathway flux by AR inhibitors (ARIs) could be a potential therapeutic opportunity [7,8]. In order to select and develop therapeutic drugs for diabetes and diabetic complications, structure-based enzyme mechanism studies have been undertaken as an effective approach. Considering enzymes and inhibitors, mutual studies of molecular docking and enzyme kinetic mechanism of RLAR can predict the potentials of ARIs as anti-diabetic complication agents.

Flavonoids are secondary metabolites that are distributed in member of the high plant kingdom such as fruits and vegetables. Due to relatively lower toxicity and a stronger bioactive potential for increase human health, especially antioxidants, there have been numerous studies based on the development of pharmaceutical drugs. Starting from the basic structure (C6-C3-C6) which is present in chalcones, flavones, flavanones, flavonols, and aurones, the structures of flavonoids are diverse and are determined by the number and arrangement of the substituents and glycosylations [21,22]. Since many flavonoids have been implicated in the alleviation of diabetic complications, many researchers have scrutinized their relevance in AR inhibition [7,23-25]. In particular, prenylated flavonoids possess additional hydrophobic and

anionic characteristic moieties (prenyl groups) on their flavonoid skeletons which may play important roles in enzyme inhibition [18]. In our previous study, the inhibitory activity of **3**, lacking a prenyl group at the C-8 position, was drastically decreased compared to those of prenylated flavonols **1** and **2**, indicating that the hydrophobic aliphatic groups may, at least in part, be associated with increased inhibitory activity [18,19]. Furthermore, the type of RLAR inhibition depended on the absence or presence of prenyl groups, in that **3** showed noncompetitive inhibition, whereas **1** and **2** are mixed inhibitors to RLAR in the present study (Figures 2 and 3). In other words, **2** and **3** can bind to both the allostatic site of the free enzyme and to the enzyme/substrate complex; **3** binds to the free enzyme and inhibits the formation of the enzyme/substrate complex. Depending on the relative values of the K_i (the dissociation constant of inhibitors), the V_{max} results of **2** and **3** possessing an additional prenyl group increased regardless of whether the substrate was bound to the enzyme.

Based on molecular docking studies, flavonoids have been shown to be widely disseminated as naturally occurring ALR2 inhibitors. Recently, there has been staggering supporting research on structure-activity relationship of flavonoids, including enzyme kinetics and molecular docking studies [26,27]. With respect to the docking modeling, the findings have unveiled that the dissociated anionic hydroxyl group at C-7 interacts with Tyr48, His110, Trp111, and the positively-charged nicotinamide ring of the $NADP^+$ cofactor in the active site cavity of ALR2. Moreover, the additional hydrophobic pocket located in the active site (Leu300 and Trp111) interacts with the C-2 benzyl substituent. The presence of a 4′-hydroxyl group on the B-ring can also increase the affinity and inhibitory potency against ALR2 via interaction with Thr113 at the active site [23,28]. Through modeling studies, the

phenoxy group has been shown to provide a good structural replacement for the carboxylate group (the most well known ARIs are tolrestat, sorbinil), which can account for the possibility of flavonoids as potent ALR2 inhibitors [8]. In fact, the specificity and selectivity of ALRs are closely related to the hydrophobic pocket of ALRs, including Leu300 and Trp111. In particular, Leu300 is the short segment of the enzyme susceptible to conformational changes, followed by the determination of the ligand specificity toward ALR2 compared to that of ALR1 [28]. Comparative molecular modeling studies of **1**~**3** revealed that all three compounds can bind tightly to the active site through Trp20, Tyr48, His110, and Trp111 residues. Unlike compound **3**, the two prenylated kaempferols **1** and **2** interact with Leu300 and Phe122 residues at a specific nonpolar site of ALR2 (Figure 4). Considering this result, the presence of the 8-prenyl group might have an important role in the selectivity and potency of ALR inhibition via strong anionic tendency at the adjacent 7-hydroxyl group as well as the 4′-hydroxyl group.

Conclusions

The docking simulation results of **1** ~ **3** demonstrating the negative binding energies (Autodock 4.0 = –9.11 to –7.64 kcal/mol; Fred 2.0 = –79.54 to –51.84 kcal/mol) and the additional hydrogen bonds through Phe122 and Trp219, in addition to the previously proposed interaction of AR and phenolics through Trp20, Tyr48, His110, and Trp111 residues, have highlighted that the presence of 8-prenyl and 5-methyl groups might potentiate tighter binding to the active site of an enzyme, making them much more effective as AR inhibitors. The present study suggested that an effective strategy for screening the potential of AR inhibitors could be established by predicting

the 3D structural conformation of prenylated flavonoids and the orientation within the enzyme, as well as by simultaneously determining the mode of enzyme inhibition. This simultaneous approach might be underlined as a potential guideline for the design of AR-selective inhibitors

Methods

General

The ^{1}H- and ^{13}C-NMR spectra were determined using a JEOL JNM ECP-400 spectrometer (Tokyo, Japan) at 400 MHz for ^{1}H and 100 MHz for ^{13}C in deuterated dimethylsulfoxide (DMSO)-d_6. Column chromatography was conducted using silica (Si) gel 60 (70–230 mesh, Merck, Darmstadt, Germany) and Sephadex LH-20 (20~100 μm, Sigma, St. Louis, MO, USA). All TLC was conducted on pre-coated Merck Kieselgel 60 F_{254} plates (20 × 20 cm, 0.25 mm, Merck) or RP-18 F_{254s} plates (5 × 10 cm, Merck), using 50% H_2SO_4 as a spray reagent.

Chemicals and reagents

β-Nicotinamide adenine dinucleotide phosphate (NADPH), DL-glyceraldehyde dimer, kaempferol, and quercetin were purchased from Sigma Chemical Co. (St. Louis, MO, USA). All solvents were purchased from Merck, Fluka, Duksan Pure Chemical Co., or Sigma Aldrich Co., unless stated otherwise.

Isolation of desmethylanhydroicaritin and sophoflavescenol

The dried roots of *S. flavescens* (10 kg) were refluxed with methanol (MeOH) for 3 h (3 × 10 L). The total filtrate was then concentrated to dryness *in vacuo* at 40 ℃ in order to render the MeOH extract (2.2 kg). This extract was successively partitioned with methylene chloride (CH_2Cl_2), ethyl acetate, *n*-butanol and water. The CH_2Cl_2-soluble fraction was chromatographed over a Si gel column with a CH_2Cl_2–MeOH mixture (gradient) and further separated by Sephadex LH-20 (solvent: MeOH) to yield desmethylanhydroicaritin (**1**, 45 mg) and sophoflavescenol (**2**, 600 mg). These compounds were characterized and identified by spectroscopic methods, including ^{1}H- and ^{13}C-NMR, as well as through comparison with published data [16,19]. The structures are shown in Figure 1, and their spectral data are as follows.

Desmethylanhydroicaritin (1) ^{1}H-NMR (400 MHz, DMSO-d_6) δ : 12.40 (1H, s, OH-5), 10.73 (1H, s, OH-7), 10.12 (1H, s, OH-4'), 9.36 (1H, s, OH-3), 8.03 (2H, d, *J* = 8.87 Hz, H-2', 6'), 6.93 (2H, d, *J* = 8.87 Hz, H- 3', 5'), 6.29 (1H, s, OH-6), 5.17 (1H, t, *J* = 6.85 Hz, H-2"), 3.42 (2H, d, *J* = 6.45 Hz, H-1"), 1.74 (3H, br s, H-4") 1.62 (3H, br s, H-5"); ^{13}C-NMR (100 MHz, DMSO-d_6) δ : 176.11 (C-4), 161.13 (C-7), 159.14 (C-4'), 158.25 (C-5), 153.44 (C-9), 146.72 (C-2), 135.49 (C-3), 130.91 (C-3"), 129.34 (C-2', 6'), 122.54 (C-2"), 121.96 (C-1'), 115.44 (C-3', 5'), 105.56 (C-8), 102.98 (C-10), 97.76 (C-6), 25.42 (C-5"), 21.19 (C-1"), 17.80 (C-4").

Sophoflavescenol (2) ^{1}H-NMR (400 MHz, DMSO-d_6) δ: 10.58 (1H, s, 7-OH), 9.99 (1H, s, 4′-OH), 7.98 (2H, d, *J* = 8.8 Hz, H-2′/H-6′), 6.91 (2H, d, *J* = 8.8 Hz, H-3′/H-5′), 6.44 (1H, s, H-6), 5.15 (1H, t-like, H-2″), 3.80 (3H, s, 5-OCH_3), 3.46 (2H, brd, *J* = 6.7 Hz, H-1″), 1.75 (3H, s, H-5″), 1.62 (3H, s, H-4″). ^{13}C-NMR (100 MHz, DMSO-d_6) δ: 171.2 (C-4), 159.5 (C-7), 158.5 (C-4′), 157.9 (C-5), 155.4 (C-9), 141.8 (C-2), 136.8 (C-3), 130.9 (C-3″), 128.6 (C-2′/ C-6′), 122.7 (C-2″), 122.3 (C-1′), 115.4 (C-3′/C-5′),

106.8 (C-8), 105.2 (C-10), 95.4 (C-6), 55.7 (5-OCH_3), 25.4 (C-4″), 21.5 (C-1″), 17.8 (C-5″).

Assay for RLAR inhibitory activity

Rat lens homogenates were used as AR sources. In the experiment, we followed the Guidelines for Care and Use of Laboratory Animals as approved by Pukyong National University (Busan, Republic of Korea). Rat lens homogenate was prepared according to the modified method of Hayman and Kinoshita [29]. Briefly, the lenses were removed from the eyes of Sprague-Dawley rats weighing 250 ~ 280 g (Samtako BioKorea, Inc.) and homogenized in sodium phosphate buffer (pH 6.2). The supernatant was obtained by centrifugation of the homogenate at 10,000 rpm at 4 °C for 20 min and was frozen until use. A crude AR, with a specific activity of 6.5 U/mg, was used in the evaluations of enzyme inhibition. The partially purified material was separated into 1.0 ml aliquots, and stored at –80 °C. Each 1.0 ml cuvette contained equal units of enzyme, 100 mM sodium phosphate buffer (pH 6.2), and 1.6 mM NADPH, both with and without 50 mM of the substrate, DL-glyceraldehyde, and an inhibitor (f.c. 100 μM for the isolated compounds, dissolved in 100% DMSO) with a final concentration of 1% DMSO. The AR activity was determined by measuring the decrease in NADPH absorption at 340 nm over a 4 min period on a Ultrospec®2100pro UV/Visible spectrophotometer with SWIFT II Applications software (Amersham Biosciences, New Jersey, USA). The inhibition percentage (%) was calculated as [(1 − (*Δ*A sample/min − *Δ*A blank/min) / (*Δ*A control/min − *Δ*A blank/min)) × 100], where *Δ*A sample/min represents the reduction of absorbance for

4 min with the test sample and substrate, respectively, and ΔA control/min represents the same but with 100% DMSO instead of a sample.

Kinetic parameters in RLAR inhibition – Dixon and Lineweaver–Burk plots

In order to determine the kinetic mechanism, two kinetic methods using Lineweaver–Burk plots and the Dixon plots were complementarily used [11-13]. Each enzymatic inhibition at various concentrations of three test compounds was evaluated by monitoring the effects of different concentrations of the substrates in Dixon plots (single reciprocal plot). Dixon plots for inhibition of RLAR were obtained in the presence of different concentrations of DL-glyceraldehyde substrate: 25 mM (●); 50 mM (○); and 100 mM (▼). The test concentrations of test flavonoids in the RLAR kinetic analysis were as follows: 0.56 and 0.11 μM for **1**; 2.78, 2.71, 0.54, and 0.11 μM for **2**; and 34.94, 17.47, and 3.49 μM for **3**. The enzymatic procedures consisted of the same, aforementioned RLAR assay methods. The inhibition constants (K_i) were determined by interpretation of the Dixon plots. By means of Lineweaver–Burk double reciprocal plots, K_m and V_{max} values of RLAR were determined at various concentrations of DL-glyceraldehyde (25, 50, and 100 mM) substrate in the absence and presence of different concentrations of test compounds (0.56 and 0.11 μM for **1**; 2.78, 2.71, 0.54, and 0.11 μM for **2**; and 34.94, 17.47, and 3.49 μM for **3)**. The K_i value was also derived by plotting slopes obtained from Lineweaver–Burk plots and Dixon plots.

Molecular docking simulation in RLAR inhibition – Autodock 4.0 and Fred 2.0

In order to estimate the conformation of the protein-ligand complex and to increase accuracy, repeatability, and reliability of the docking results, two programs: Autodock 4.0 (AutoDock4 and AutoDockTools4) and Fred 2.0 (OpenEye Scientific Software, Santa Fe, NM, USA) were utilized. Twelve ligand structures were constructed and minimized using Chemsketch 3.5 and Omega 2.0 software (OpenEye Scientific Software, USA), for 2D and 3D conformation, respectively [30]. For docking studies, the crystal structures of the protein targets (NCBI protein ID : NP_001619.1) were allocated from the protein sequence alignment [Brookhaven Protein Data Bank (PDB ID: 2acr chain A)]. The 3D structures of test compounds are as follows: desmethylanhydroicaritin (PUBCHEM ID: 5318624); sophoflavescenol (PUBCHEM ID : 9929189); and kaempferol (PUBCHEM ID: 5280863). The predicted protein ligand complexes were optimized and ranked according to the empirical scoring function, ScreenScore, which estimates the binding free energy of the ligand receptor complex. The docking of the aldose reductase-flavonoid molecule was successful, as indicated by statistically significant scores.

Statistics

Statistical significance was analyzed by one-way ANOVA and Student's *t*-test (Systat Inc., Evanston, IL, USA) and considered significant at $p < 0.01$. All results are presented as mean ± SEM.

Acknowledgements

This work was financially supported by the Blue-Bio Industry RIC at Dong-Eui University as an RIC program of ITEP under MKE and Busan City and by a National

Research Foundation of Korea grant funded by the Korean government (E00755). This research was also partially assisted by the Korean Bioinformation Center (KOBIC) Research Support Program.

Authors' contributions

HAJ and JSC carried out the design, coordination, and analysis of overall bioactive assays, enzyme kinetics, and molecular docking studies, and drafted and corrected the manuscript. HEM and SHO participated in the performance and analysis of the individual study. BWK, HSS, SBK conceived of the study, and participated in its coordination and helped to review the manuscript. All authors read and approved the final manuscript.

References

1. El-Kabbani O, Ruiz F, Darmanin C, Chung RP: **Aldose reductase structures: implications for mechanism and inhibition.** *Cell Mol Life Sci* 2004, **61:** 750-762.
2. Brownlee M: **Biochemistry and molecular cell biology of diabetic complications.** *Nature* 2001, **414:** 813-820.
3. Nishimura C, Yamaoka T, Mizutani M, Yamashita K, Akera T, Tanimoto T: **Purification and characterization of the recombinant human aldose reductase expressed in baculovirus system.** *Biochim Biophys Acta* 1991, **1078:** 171-178.

4. Kubo E, Miyoshi N, Fukuda M, Akagi Y: **Cataract formation through the polyol pathway is associated with free radical production.** *Exp Eye Res* 1999, **68:** 457-464.
5. Lee AY, Chung SS: **Contributions of polyol pathway to oxidative stress in diabetic cataract.** *FASEB J* 1999, **13:** 23-30.
6. Kador PF, Kinoshita JH, Tung WH, Chylack LT Jr: **Differences in the susceptibility of various aldose reductases to inhibition. II.** *Invest Ophthalmol Vis Sci* 1980, **19:** 980-982.
7. Kawanishi K, Ueda H, Moriyasu M: **Aldose reductase inhibitors from the nature.** *Curr Med Chem* 2003, **10:** 1353-1374.
8. de la Fuente JA, Manzanaro S, Martín MJ, de Quesada TG, Reymundo I, Luengo SM, Gago F: **Synthesis, activity, and molecular modeling studies of novel human aldose reductase inhibitors based on a marine natural product.** *J Med Chem* 2003, **46:** 5208-5221.
9. El-Kabbani O, Podjarny A: **Selectivity determinants of the aldose and aldehyde reductase inhibitor-binding sites.** *Cell Mol Life Sci* 2007, **64:** 1970-1978.
10. El-Kabbani O, Old SE, Ginell SL, Carper DA: **Aldose and aldehyde reductases: structure-function studies on the coenzyme and inhibitor-binding sites.** *Mol Vis* 1999, **5:** 20.
11. Lineweaver H, Burk D: **The determination of enzyme dissociation constants.** *J Am Chem Soc* 1934, **56:** 658-666.
12. Cornish-Bowden A: **A simple graphical method for determining the inhibition constants of mixed, uncompetitive and non-competitive inhibitors**. *Biochem J* 1974, **137:** 143-144.

13. Dixon M: **The determination of enzyme inhibitor constants.** *Biochem J* 1953, **55:** 170-171.

14. Morris GM, Huey R, Lindstrom W, Sanner MF, Belew RK, Goodsell DS, Olson AJJ: **AutoDock4 and AutoDockTools4: Automated docking with selective receptor flexibility.** *J Comput Chem* 2009, **30:** 2785-2791.

15. Bustanji Y, Al-Masri IM, Qasem A, Al-Bakri AG, Taha MO: **In silico screening for non-nucleoside HIV-1 reverse transcriptase inhibitors using physicochemical filters and high-throughput docking followed by in vitro evaluation.** *Chem Biol Drug Des* 2009, **74:** 258-265.

16. Jung HJ, Kang SS, Hyun SK, Choi JS: ***In vitro*** **free radical and $ONOO^-$ scavengers from *Sophora flavescens*.** *Arch Pharm Res* 2005, **28:** 534-540.

17. Jung HA, Jeong DM, Chung HY, Lim HA, Kim JY, Yoon NY, Choi JS: **Re-evaluation of the antioxidant prenylated flavonoids from the roots of *Sophora flavescens*.** *Biol Pharm Bull* 2008, **31:** 908-915.

18. Jung HA, Yoon NY, Kang SS, Kim YS, Choi JS: **Inhibitory activities of prenylated flavonoids from *Sophora flavescens* against aldose reductase and generation of advanced glycation endproducts.** *J Pharm Pharmacol* 2008, **60:** 1227-1236.

19. Jung HA, Jin SE, Park JS, Choi JS: **Antidiabetic complications and anti-Alzheimer activities of sophoflavescenol, a prenylated flavonol from *Sophora flavescens*, and its structure-activity relationship.** *Phytother Res* 2011, **25:** 709-715.

20. de Groot M, Anderson R, Freedland KE, Clouse RE, Lustman PJ: **Association of depression and diabetes complications: a meta-analysis.** *Psychosom Med* 2001, **63:** 619-630.

21. Rice-Evans CA, Miller N, Paganga G: **Structure-antioxidant activity relationships of flavonoids and phenolic acids.** *Free Radic Biol Med* 1996, **20:** 933-956.

22. Harborne FB, Williams CA: **Advances in flavonoid research since 1992.** *Phytochemistry* 2000, **55:** 481-504.

23. Nicolle E, Souard F, Faure P, Boumendjel A: **Flavonoids as promising lead compounds in type 2 diabetes mellitus: molecules of interest and structure-activity relationship.** *Curr Med Chem* 2011, **18:** 2661-2672.

24. Matsuda H, Morikawa T, Toguchida I, Yoshikawa M: **Structural requirements of flavonoids and related compounds for aldose reductase inhibitory activity.** *Chem Pharm Bull* 2002, **50:** 788-795.

25. Lim SS, Jung YJ, Hyun SK, Lee YS, Choi JS: **Rat lens aldose reductase inhibitory constituents of *Nelumbo nucifera* stamens.** *Phytother Res* 2006, **20:** 825-830.

26. Fernández M, Caballero J, Helguera AM, Castro EA, González MP: **Quantitative structure-activity relationship to predict differential inhibition of aldose reductase by flavonoid compounds.** *Bioorg Med Chem* 2005, **13:** 3269-3277.

27. Mercader AG, Duchowicz PR, Fernández FM, Castro EA, Bennardi DO, Autino JC, Romanelli GP: **QSAR prediction of inhibition of aldose reductase for flavonoids.** *Bioorg Med Chem* 2008, **16:** 7470-7476.

28. Miyamoto S: **Molecular modelling and structure-based drug discovery studies of aldose reductase inhibitors.** *Chem-Bio Informatics Journal* 2002, **2:** 74-85.

29. Hayman S, Kinoshita J H: **Isolation and properties of lens aldose reductase.** *J Biol Chem* 1965, **240:** 877-882.

30. Harrison DH, Bohren KM, Ringe D, Petsko GA, Gabbay KH: **An anion binding site in human aldose reductase: mechanistic implications for the binding of citrate, cacodylate, and glucose 6-phosphate.** *Biochemistry* 1994, **33:** 2011-2020.

Figure legends

Figure 1 Structures of test compounds 1~3

Figure 2 Dixon plots for RLAR inhibition of compounds 1~3

Desmethylanhydroicaritin (A), sophoflavescenol (B), and kaempferol (C) were tested in the presence of different concentrations of substrate (DL-glyceradehyde): 25 mM (●); 50 mM (○); and 100 mM (▼).

Figure 3 Lineweaver-Burk plots for RLAR inhibition of compounds 1~3

RLAR inhibition was analyzed in the presence of different concentrations of sample as follows: 0 μM (●), 0.11 μM (○), and 0.56 μM (▼) for desmethylanhydroicaritin (A); 0 μM (●), 0.108 μM (○), 0.54 μM (▼), and 2.71 μM (▽) for sophoflavescenol (B); 0 μM (●), 17.47 μM (○), and 34.94 μM (▼) for kaempferol (C).

Figure 4 Molecular docking models for RLAR inhibition of compounds 1~3

desmethylanhydroicaritin (A), sophoflavescenol (B), and kaempferol (C)

Table 1 IC_{50} values and dissociation constants (K_i) of compounds 1~3 for RLAR activity using the Dixon plot

Test compound	IC_{50} (μM)	K_i (μM)	Inhibition type
1	1.03 ± 0.13	0.94	mixed
2	0.76 ± 0.04	0.69	mixed
3	5.13 ± 0.05	4.65	noncompetitive

Table 2 Kinetic parameters of compounds 1~3 regarding RLAR activity according to the Lineweaver-Burk plot

Test compound	Conc. (μM)	K_i (μM)	K_m (mM)	V_{max} (μmole/mL/min)	Inhibition type
1	0.00		8.20 ± 0.04	0.016 ± 0.002	mixed
	0.11	0.52	9.84 ± 0.05	0.014 ± 0.002	
	0.56	0.63	12.32 ± 0.08	0.010 ± 0.001	
2	0.00		11.48 ± 0.07	0.016 ± 0.002	mixed
	0.11	0.41	12.14 ± 0.05	0.013 ± 0.001	
	0.54	0.37	13.38 ± 0.08	0.010 ± 0.000	
3	0.00		40.10 ± 0.12	0.026 ± 0.001	noncompetitive
	17.47	6.30	40.11 ± 0.15	0.007 ± 0.000	
	34.94	6.20	40.11 ± 0.14	0.004 ± 0.000	

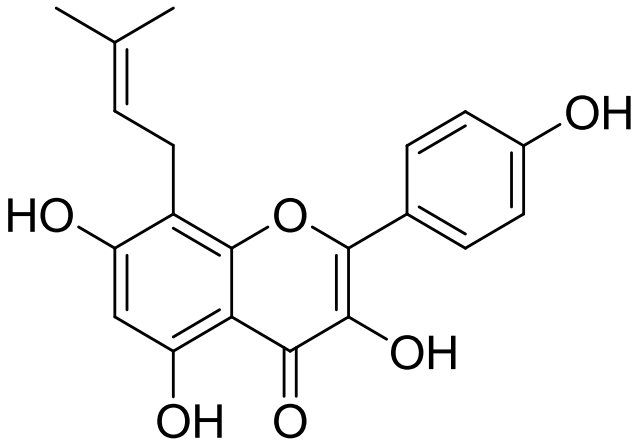

desmethylanhydroicaritin

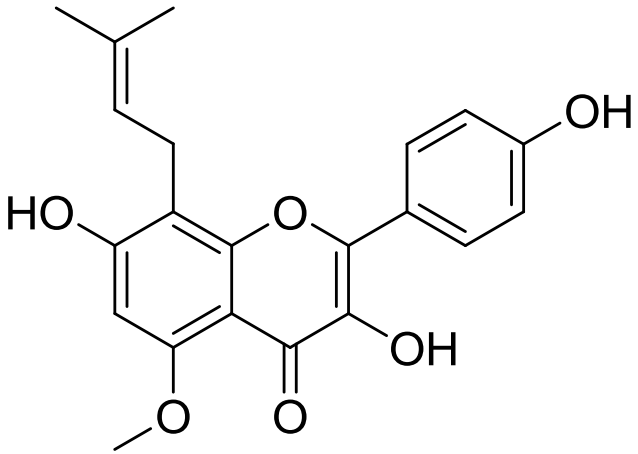

sophoflavescenol

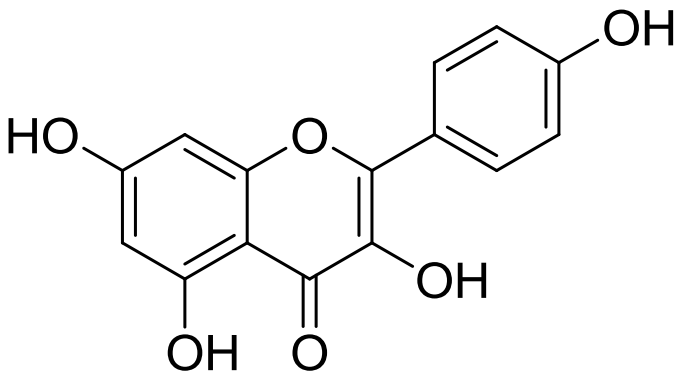

kaempferol

Figure 1

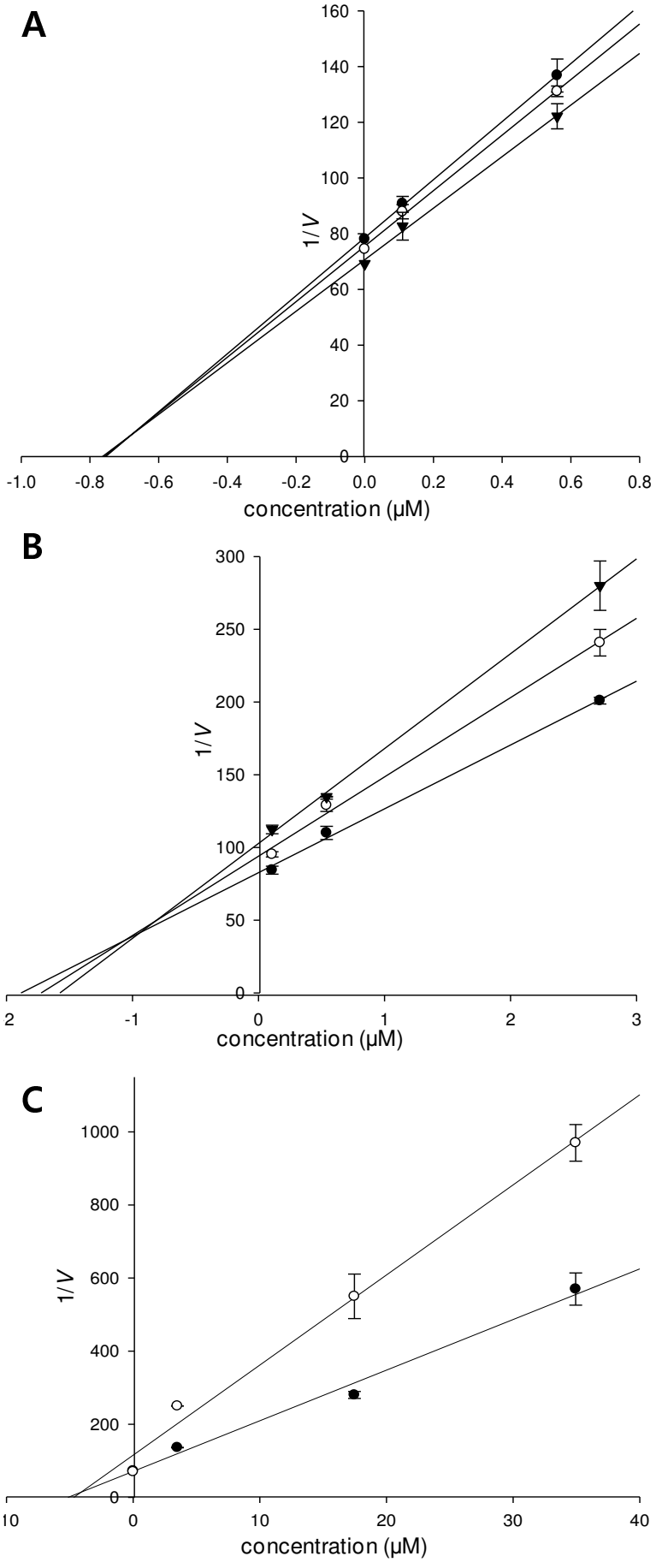
A
160
140
120
100
80
60
40
20
0
1/V
-1.0
-0.8
-0.6
-0.4
-0.2
0.0
0.2
0.4
0.6
0.8
concentration (μM)
B
300
250
200
150
100
50
0
1/V
2
-1
0
1
2
3
concentration (μM)
C
1000
800
600
400
200
0
1/V
10
0
10
20
30
40
concentration (μM)

Figure 2

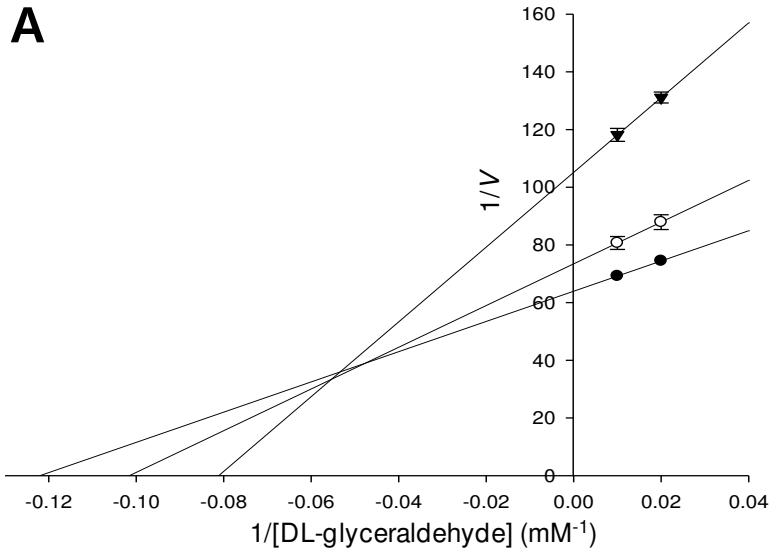
A
160
140
120
100
80
60
40
20
0
1/V
-0.12
-0.10
-0.08
-0.06
-0.04
-0.02
0.00
0.02
0.04
1/[DL-glyceraldehyde] (mM-1)

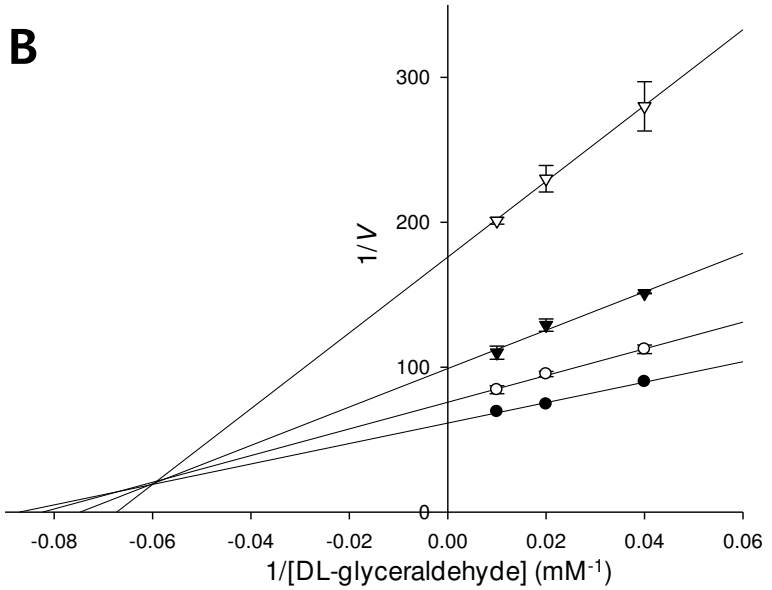
B
300
200
100
0
1/V
-0.08
-0.06
-0.04
-0.02
0.00
0.02
0.04
0.06
1/[DL-glyceraldehyde] (mM-1)

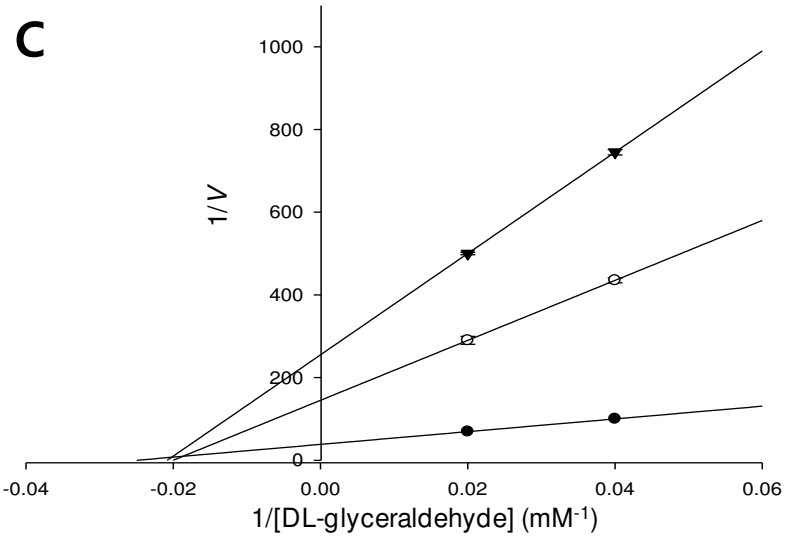
C
1000
800
600
400
200
0
1/V
-0.04
-0.02
0.00
0.02
0.04
0.06
1/[DL-glyceraldehyde] (mM-1)

Figure 3

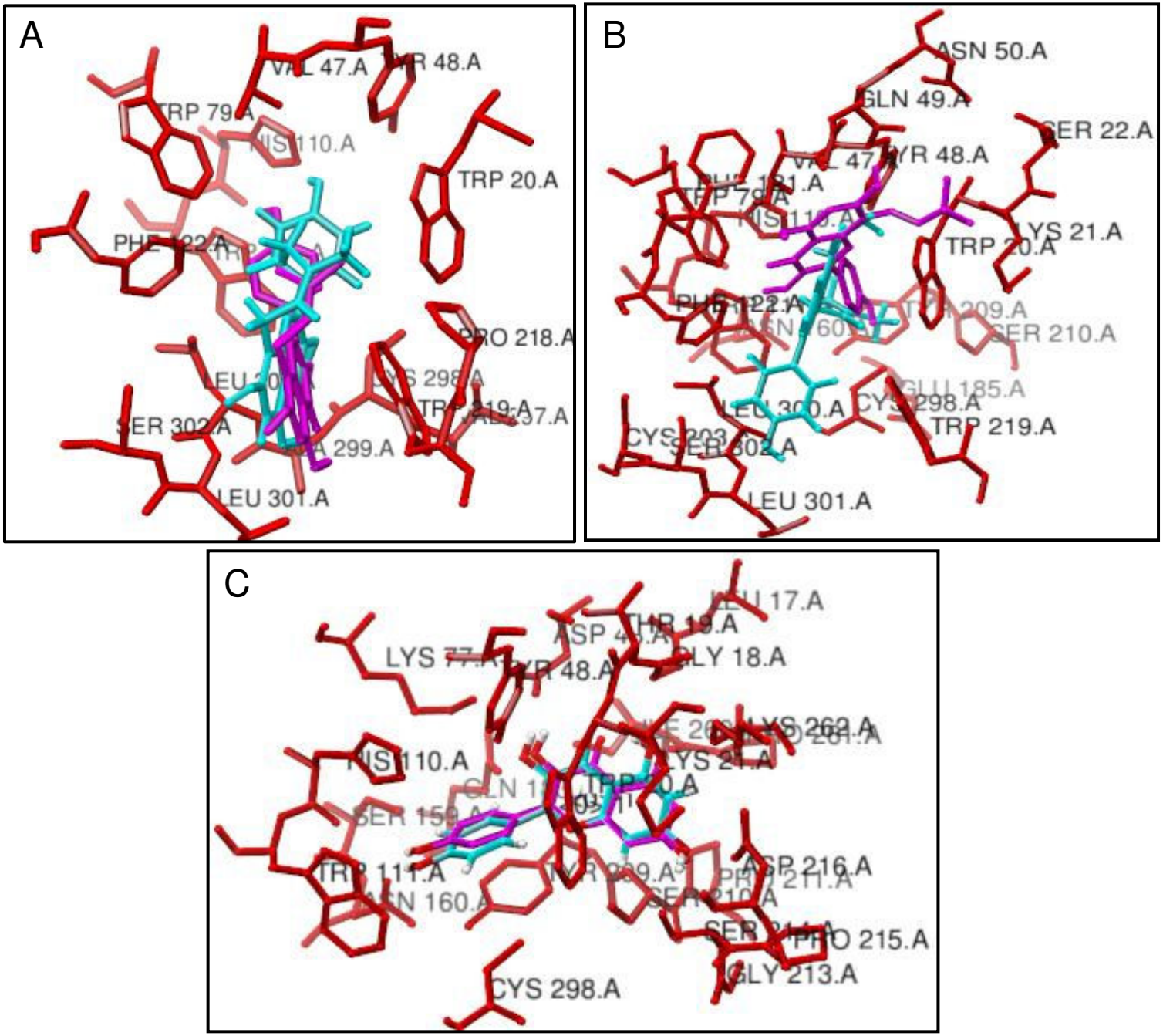
A
TRP 20.A
PRO 218.A
SER 302.A
LEU 301.A
B
ASN 50.A
SER 22.A
LYS 21.A
TRP 20.A
SER 210.A
TRP 219.A
CYS 203.A
SER 302.A
LEU 301.A
C
LYS 298.A

Figure 4